VI Data processing and results of the FROG field campaign. Inter-comparison with theoretical models

VI.1 Introduction

First of all, a brief explanation of the FROG radiometric and foam surface coverage measurements, as well as the vertical profile image processing is given. Second, the foam emissivity measurements and their dependence with: SSS, incidence angle, polarization are presented, as well as the emissivity of the sea surface roughed by artificially generated rain. Third, an inter-comparison between the FROG results and a two-layer theoretical foam model [24] and [25] using the experimental data as inputs is presented. Finally, an inter-comparison between the FROG results and the theoretical predictions of the emission of the sea surface roughed by rain is presented [50].

VI.2 Data processing

VI.2.1 Raw data pre-processing

Raw data was acquired using:

a) the industrial PC to save the radiometric, meteorological and surface foam coverage images from the SONY SSC-DC393 video camera simultaneously,

b) a second PC, to save the foam vertical profile from the Ultrak KC550xCP, and

c) the data logger to save the data from the temperature sensors needed to measure the water surface temperature.

Additional information from the Deltebre meteorological station, and SSS from the IRTA's salinometer were also acquired.

Radiometric and meteorological data were collected at a rate of one second. Meteorological data from Deltebre station were acquired every 30 minutes, and temperature sensors saved at a rate of one sample per minute.

The radiometric data were continuously saved using the naming and structure described in the following paragraphs. For each new date, a directory named `yyyymmdd` is created, which contains all the files generated in this date. At the end of each day during the field experiment, all files included in this directory were copied to a CD-Rom as a backup and for later processing. The schematic file structure is:

```
[rootdir]
    yymmdd                          (data directory)
        raw                         (raw data directory)
            yymmdd[NN].rad          (radiometric data file)
```

`yymmdd.txt` (historic data file)

where [NN] is a two-digit sequential number starting at 00 each day. All data files are ASCII files, and they contain an indefinite number of lines, each one corresponding to a single measurement, and different fields in each line. A brief description of the fields for all data files is given in the following paragraphs.

a) Radiometric data file: this file contains the radiometer's output, the digital clinometer, the meteorological data, as well as information on the radiometer physical temperature. In order to avoid huge files, several ones are created automatically, being [NN] the sequential number. A new file can be created for several reasons: 1) maximum size is limited to 5,000 lines (~900 KBytes), 2) start a new sequence, or 3) the sequence process has been aborted. The fields are divided in to the next parameters:

- Julian day (number of days within the year),
- GPS UTC time (hours, minutes and seconds) at 1 sec interval,
- operation mode[3]: measurements (0), hot load calibration (1), cold load calibration (2), software temperature control (3),
- radiometer position: given by the step motor (elevation and azimuth position),
- clinometers pitch: to correct for instrument's incidence angle oscillations due to e.g. wind,
- vertical and horizontal receivers detector output voltages (V_H, V_V),
- digital correlator counts (for *U* and *V* parameters),
- output voltages of internal temperature sensors (T_{refH}, T_{refV}, T_{int}, T_{ph_corr}),
- output voltages of external temperature sensors (T_{ext}),
- temperature from UPC meteorological sensors (Case, T_{ph_abs}, T_{ms_ext}, T_{ms_int}),
- humidity from UPC meteorological sensors (RH_{ext}, RHi_{nt}),
- wind speed and wind direction from UPC meteorological anemometer and weathervane (WS, WD),
- rain counts from the UPC rain gauge,
- pressure from the UPC station, and
- control signal (information about the PID control, chapter II).

b) Historic data: this file contains information about the movements of the radiometer. Contains the Julian day, the GPS UTC time, and the azimuth and elevation position when the instrument has moved.

[3] When operation mode is selected to 3 radiometric data is not acquired

All data are formatted according to the radiometric data. The raw data are classified depending on the type of sequence described in chapter V.

VI.2.2 Radiometric data processing

A set of routines were programmed to obtain the final data. Each sequence is composed by two calibrations at the beginning and at the end of each cycle, and the measurement selected between five types is explained in chapter V.

FROG data processing consisted of deriving the first two Stokes parameters (T_H and T_V) taking into account the following considerations, depending on the type of measurement:

- Water, oil and rain measurements: as shown in chapter V, the Dicke radiometer's output voltage is proportional to the antenna's temperature. The voltage "a" and the offset "b" are obtained in the same manner as in the WISE data processing. In other words, as T_{abs} and T_{sky} are well-known, and V_H and V_V are the measured detector output voltages of H- and V-channels, "a" and "b" parameters can be readily obtained. The mean value and the standard deviation define the data collected by the radiometer. The data samples values that deviate more than 3σ are eliminated being suspicious of RFI or contamination, and the mean and the standard deviation of the current samples are calculated again. T_B is divided into three terms: a) the first one is the mean value, b) another effect that it is necessary to take into account is the contribution of the atmospheric downward emission (T_{DN}) reflected on the water surface, that depends on the incidence angle, c) the last term refers to the correction applied to the measurements due to the antenna finite beamwidth effects (chapter IV). Finally, to avoid the physical temperature dependence, the emissivity is calculated as in the eqn. (6.1).

$$e = \frac{T_B}{T_{surf}} \quad , \tag{6.1}$$

- Foam measurements: as seen in chapter V, this type of measurement was taken the following sequence: no foam, foam, and no foam. Hence, the process to obtain the T_B referred to the no-foam measurements is identical to the water measurements process. Emissivity foam sequences are explained in the following sections. Foam emissivity values of each sequence are normalized, for a patch completely covered by foam.

The output files are classified according to the type of measurement. Each file is named following the nomenclature: `type_n[N]_S[NN]_f[NNN]`, where `type` is the type of measurement, `n[N]` is the number of repetitions, `S[NN]` is the salinity concentration, `f[NNN]` is the initial estimated foam coverage (25 %, 50 % or 100 %). The fields are divided in the next parameters:

- Julian day (number of days within the year),
- Start and finish of each sequence (hour, minutes, seconds).
- Radiometer position: given by the step-by-step motor, (elevation position),
- T_H and T_V *mean* and *std* values,
- T_{sky}, and
- Sea surface salinity and Sea surface temperature.

VI.2.3 Foam data processing

First of all, foam coverage data files are composed of video data and they are saved simultaneously with the radiometric data. As the video sequence started and finished at the beginning and end of each sequence, snapshots corresponding to the no foam sequences must be eliminated. To reduce the computational cost and the volume of the saved information, first of all one snapshot every ten seconds was captured in grey scale, and a Motion Wavelets lossless compression codec was applied. On the other hand, the frame resolution was set to a 288x384 pixels, and frames were marked with the time of the day and date. The final foam coverage files (text files), consisted of a set of foam coverage mean values at each different incident angles. These mean foam coverage values are then assembled with the radiometric data. Foam coverage files are saved in the corresponding directories according with the data and the initial foam coverage estimate (25%, 50%, 100%), `f[NNN]`. Normally, every night two full foam measurement sequences were acquired.

Foam vertical profiles are analyzed separately from the radiometric data. Due to the huge volume of information, sequences were stored in different files depending on the incidence angle. One snapshot every three seconds was captured. The frame resolution was set to 640x480 pixels to be able to image individual bubbles and derive their properties. As in the foam coverage acquisition, gray scale frames were taken, and the Motion Wavelets codec was used to reduce the amount of information.

VI.3 The two-layer theoretical model

According to [25], $T_{B_{h,v}}^{Foam}$ is a function of following parameters: the electromagnetic frequency (f_o), the incidence angle (θ), the polarization (p), the physical temperature (T_{surf}), the average bubble radius (r_p), the bubble's water coating thickness (δ), the bubble's packing coefficient, the stickiness (κ), the foam layer thickness (d), and the air fraction beneath the foam layer (f_a).

Considering a two-layer model (Figure 6.1) and neglecting scattering effects, the brightness temperature of the foam-water system is computed according to [25] as:

$$T_{B_{H,V}}(\theta_i) = T_{surf} \cdot \left(1 - \left|\Gamma_{H,V}(\theta)\right|^2\right), \tag{6.2}$$

where $\Gamma_{H,V}$ is the spectral reflection coefficient that can be written as:

$$\Gamma_{H,V} = \frac{\Gamma_{H,V}^{01}(\theta)\cdot e^{-j\cdot 2\cdot\varphi} + \Gamma_{H,V}^{12}(\theta)}{e^{-j\cdot 2\cdot\varphi} + \Gamma_{H,V}^{01}(\theta)\cdot\Gamma_{H,V}^{12}(\theta)}, \tag{6.3}$$

where φ the attenuation factor of the foam layer that can be expressed as:

$$\varphi = \frac{\pi\cdot d}{\lambda}\cdot\frac{\left(\sqrt{\varepsilon_f^{'2}+\varepsilon_f^{''2}}+\varepsilon_f^{'}-j\cdot\varepsilon_f^{''}\right)}{\left(\sqrt{\frac{1}{2}\cdot\sqrt{\varepsilon_f^{'2}+\varepsilon_f^{''2}}+\varepsilon_f^{'}-\sin^2(\theta)}\right)}, \tag{6.4}$$

where ε_f is the complex permittivity of the region 1 expressed as:

$$\varepsilon_f = \varepsilon_f^{'} - j\cdot\varepsilon_f^{''}, \tag{6.5}$$

and λ is the electromagnetic wavelength.

On the other hand $\Gamma_{H,V}^{01}$, the Fresnel reflection coefficient between region 0 and 1, $\Gamma_{H,V}^{12}$ the Fresnel reflection coefficient between region 1 and 2 that depends on the polarization, the incidence angle an the complex permittivity, and can be written as:

$$\Gamma_H^{01}(\theta) = \frac{\cos(\theta)-\sqrt{\varepsilon_f-\sin^2(\theta)}}{\cos(\theta)+\sqrt{\varepsilon_f-\sin^2(\theta)}}, \tag{6.6}$$

$$\Gamma_V^{01}(\theta) = \frac{\varepsilon_f\cdot\cos(\theta)-\sqrt{\varepsilon_f-\sin^2(\theta)}}{\varepsilon_f\cdot\cos(\theta)+\sqrt{\varepsilon_f-\sin^2(\theta)}}, \tag{6.7}$$

$$\Gamma_H^{12}(\theta) = \frac{\sqrt{\varepsilon_f-\sin^2(\theta)}-\sqrt{\varepsilon_w-\sin^2(\theta)}}{\sqrt{\varepsilon_f-\sin^2(\theta)}+\sqrt{\varepsilon_w-\sin^2(\theta)}}, \tag{6.8}$$

$$\Gamma_V^{12}(\theta) = \frac{\varepsilon_W\cdot\sqrt{\varepsilon_f-\sin^2(\theta)}-\varepsilon_f\cdot\sqrt{\varepsilon_w-\sin^2(\theta)}}{\varepsilon_W\cdot\sqrt{\varepsilon_f-\sin^2(\theta)}+\varepsilon_f\cdot\sqrt{\varepsilon_w-\sin^2(\theta)}}, \tag{6.9}$$

where ε_W is the permittivity of the region 2 expressed as [25]:

$$\varepsilon_W = \varepsilon_{SW}\cdot\frac{1+2\cdot f_a\cdot y}{1-f_a\cdot y}, \tag{6.10}$$

where

$$y = \frac{1-\varepsilon_{SW}}{1+2\cdot\varepsilon_{SW}}\,. \tag{6.11}$$

According to [25], the foam permittivity can be expressed as:

$$\varepsilon_f = \frac{1+\frac{8}{3}\cdot\pi\overline{N_\alpha}}{1-\frac{4}{3}\cdot\pi\overline{N_\alpha}}\,, \tag{6.12}$$

and

$$\overline{N_\alpha} = \frac{\kappa\cdot\int\alpha(r)\cdot pdf(r)\cdot dr}{\frac{4}{3}\cdot\int r^3\cdot pdf(r)\cdot dr}\,, \tag{6.13}$$

where r is the bubbles radius, with a most probably radius from r_p, (peak of radii pdf) and

$$\alpha(r) = r^3\cdot\frac{(\varepsilon_W-1)\cdot(2\cdot\varepsilon_W+1)\cdot(1-q^3)}{(\varepsilon_W+2)\cdot(2\cdot\varepsilon_W+1)\cdot(1-q^3)+9\cdot\varepsilon_W\cdot q^3} \tag{6.14}$$

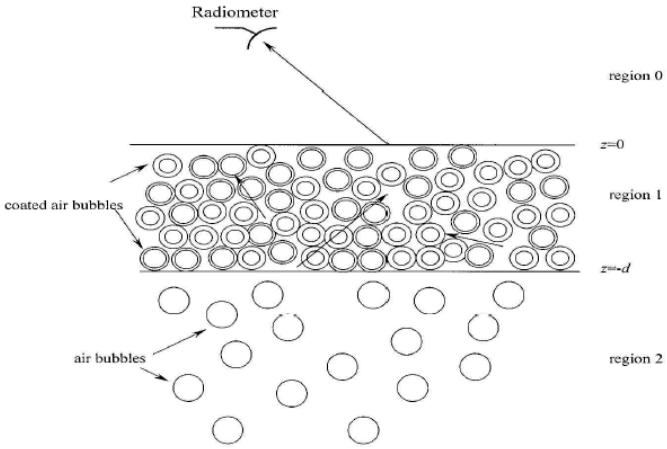

Figure 6.1. Geometrical configuration for thermal emission from foam covered ocean. The foam layer is region 1 and it is absorptive. Region 2 is air bubbles embedded in sea water and it is absorptive [24].

VI.4 FROG results. Foam contribution to the T_B measurement

The sea brightness temperature at H and V polarizations measured can be written as [37], eqn. (6.15):

$$T_{B_{H,V}}^{Total}(\theta) = F(U_{10}) \cdot T_{B_{H,V}}^{Foam} + [1 - F(U_{10})] \cdot T_{B_{H,V}}^{Water} \quad , \tag{6.15}$$

where:

- $F(U_{10})$ is the fractional sea foam coverage, which is usually parameterized in terms of the 10 m height wind speed (U_{10}) although it is known that it depends on the air-sea temperature difference, the salinity, the fetch, etc,
- θ is the incidence angle, and
- $T_{B_{H,V}}^{Foam}$ and $T_{B_{H,V}}^{Water}$ are the brightness temperatures of 100 % foam-covered and foam-free, respectively.

In the FROG 2003 field experiment the foam generation is not depend on U_{10}, but by the water salinity and the air flux pumped through the net of diffusers.

Foam is composed by a mixture of air bubbles and water generated by the breaking of the sea. According to [25] the brightness temperature increase, not only depends on the fractional area of the spot measured by the radiometer. Moreover it is necessary to take into account the volumetric distribution and the type of foam formations.

The water emissivity at L-band decreases with increasing SSS at both polarizations. This fact could be clearly observed in FROG 2003 measurements as it is shown in Figure 6.2. The θ = 20° and 55° are not considered because the radiometer collected some residual radiation from the pool walls through the secondary lobes.

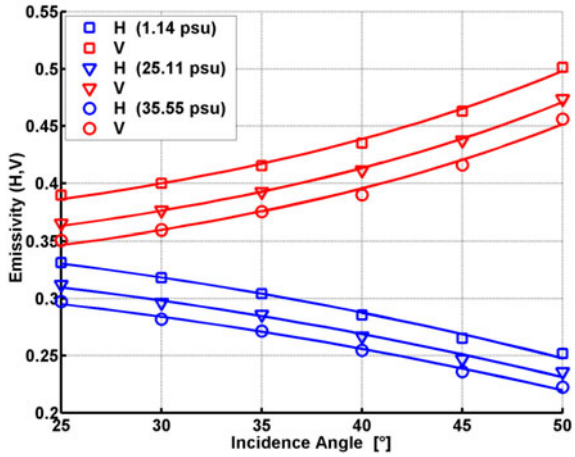

Figure 6.2. Measured emissivity (squares, triangles, and circles) at L-band at H- and V- polarizations at different salinity concentrations. Solid lines represent the specular sea surface model at the same salinities.

VI.4.1 Experimentally-derived sea water foam brightness temperature

Two corrections are applied to the measured brightness temperature ($T_{B_{H,V}}^{measured}$). The first term is the down-welling radiation (T_{DN}) (including atmospheric, cosmic and galactic noises) reflected by the surface. The second term is due to the finite antenna's beamwidth ($T_{B_{H,V}}^{finite\ beam}$) that produces a small angular averaging and a small mixing of the Stokes parameters (T_H, T_V, U, and V). Simulation results for LAURA's antenna pattern (including secondary lobes) show a constant residual bias between the antenna temperature and the brightness temperature of the sea, temperature or wind speed. Hence, the corrected brightness temperature ($T_{B_{H,V}}^{c}$) taking into account eqn. (6.16), can be expressed as:

$$T_{B_{H,V}}^{c}(\theta) = T_{B_{H,V}}^{measured} - \left[1 - e_w - F\cdot(e_f - e_w)\right]\cdot T_{DN} + T_{B_{H,V}}^{finite\ beam} \quad , \tag{6.16}$$

The impact of these two terms in $T_B^{measured}$ is small. Since the foam-induced brightness is moderate at L-band (Table 6.2), eqn. (6.16) simplifies to:

$$T_{B_{H,V}}^{c}(\theta) \cong T_{B_{H,V}}^{measured} - (1 - e_w)\cdot T_{DN} + T_{B_{H,V}}^{finite\ beam} \quad , \tag{6.17}$$

where it has been assumed that $F\cdot(e_f - e_w) << (1 - e_w)$ in the T_{DN} term.

To eliminate the dependence with the water surface temperature (T_{surf}), the foam emissivity at both polarizations has been expressed in terms of emissivity:

$$e_{H,V}^{c} = \frac{1}{F\cdot T_{surf}}\cdot T_{B_{H,V}}^{c} + \frac{1}{F\cdot T_{surf}}\cdot T_{B_{H,V}}^{water}(F-1), \tag{6.18}$$

where $T_{B_{H,V}}^{water}$ is the foam-free water corrected brightness temperature.

In Figure 6.3a and Figure 6.3b the instantaneous brightness temperature at H- and V polarizations at different incidence angles and salinities are plotted. In Figure 6.3c and Figure 6.3d the sequences' emissivity at vertical (red) and horizontal (blue) polarization are presented, for different percentage foam covers.

For these two sequences, the foam emissivity values at H- and V- polarization are presented in Table 6.1. To eliminate the foam coverage dependence, eqn. (6.18) was applied for each sequence.

Table 6.1. Foam emissivity at H- and V- polarizations.

Incidence angle θ / SSS	25°/ 33.21 psu	50°/ 33.21 psu	25°/ 37.33 psu	50°/ 37.33 psu
e_H	0.426	0.294	0.365	0.271
e_V	0.445	0.58	0.395	0.555

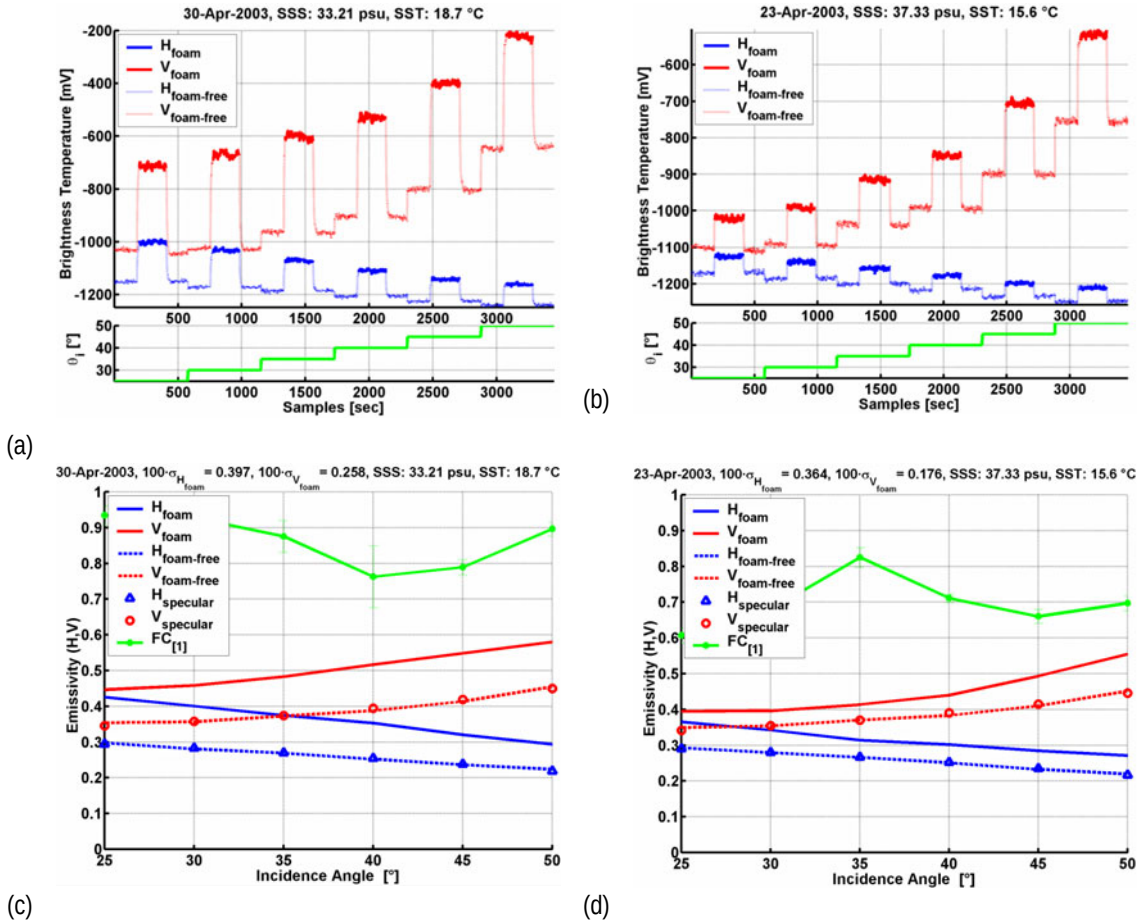

Figure 6.3. Laura radiometric raw data. H- and V- polarization: foam patch (blue/red solid line), foam-free patch (blue/red dotted line), (a) SSS = 33.21 psu, (b) SSS = 37.33 psu. L-band emissivity at H- and V- polarization: foam patch (blue/red solid line), foam-free patch (blue/red dashed line), specular water surface theoretical model (blue/red triangles/circles) (c) SSS = 33.21 psu, mean foam 86.4% (green line), and (d) SSS = 37.33 psu, mean foam 69.7% (green line).

VI.4.2 Sea water foam structure parameters measurement

In addition to the foam surface coverage needed to estimate the foam emissivity from the measurements, modelling foam emission requires the knowledge of: the foam radii distribution, the foam layer thickness, the air fraction beneath the foam layer, the bubbles' water coat thickness, and the stickyness parameter.

VI.4.2.1 Bubbles radii measurement

The bubbles radii are one of the parameters that contribute to the foam emissivity because it is an indicator of the air-water fraction content inside the foam layer. A set of vertical profiles snapshots were acquired using a video camera mounted inside a periscope for a wide range of salinities. In general at low salinities, the number of bubbles is smaller, and bubbles' radii are larger than at higher salinities. The particles structure is considered approximately spherical at salinities higher than 10 psu, shaping irregular polyhedral at lower salinities. Figure 6.4a to Figure 6.4h show 8 of vertical profiles pictures at 8 different salinities. In Figure 6.4i a detail of natural bubbles of the sea surface is shown (photograph acquired in the

Gran Canaria coast), and in Figure 6.5a to Figure 6.4h the corresponding bubbles radii pdf distribution $p_f(r)$ from FROG field experiment are shown at various salinity levels.

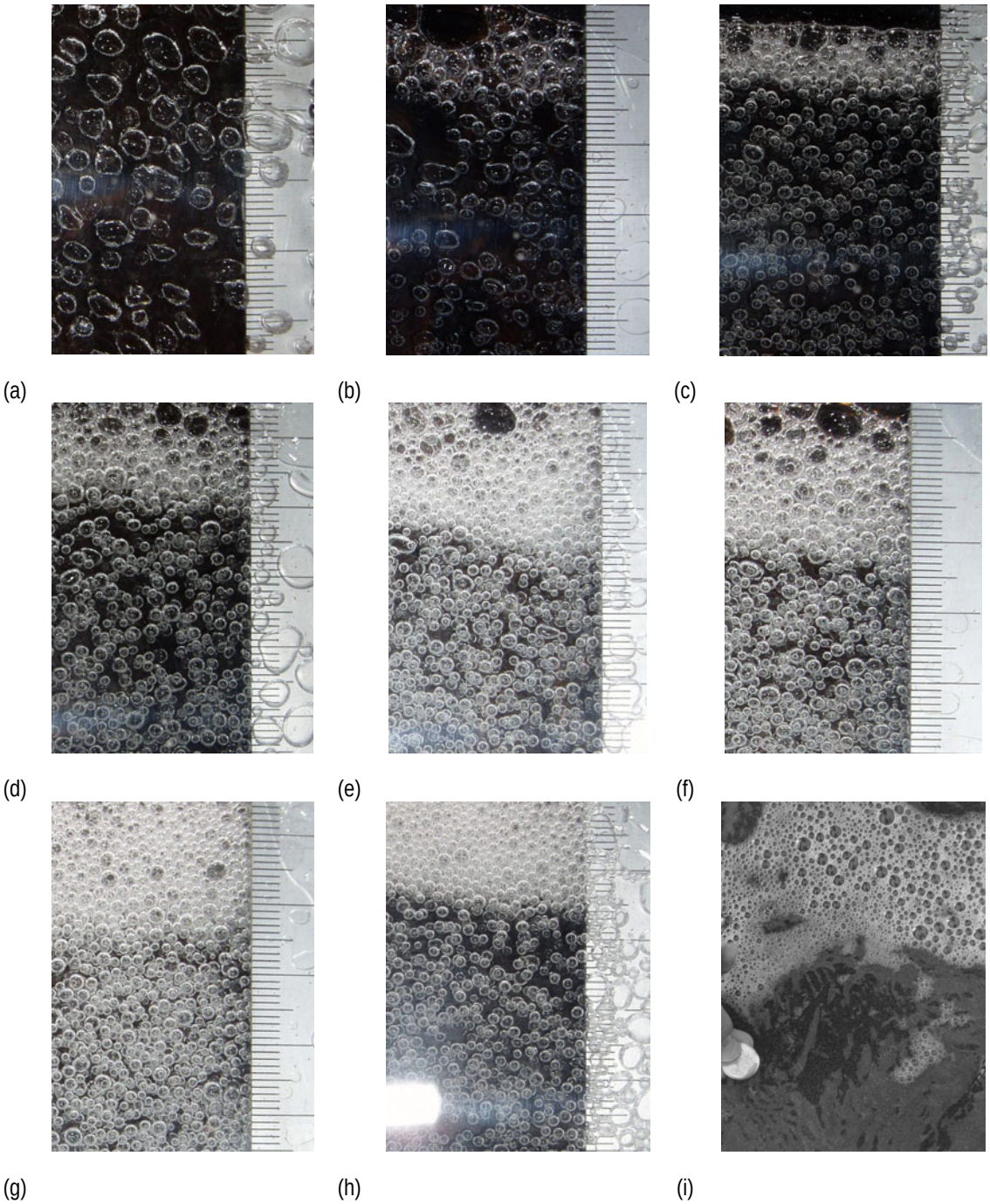

Figure 6.4. Foam vertical profiles at different salinities: (a) 0 psu, (b) 5 psu, (c) 10 psu, (d) 15 psu, (e) 20 psu, (f) 25 psu, (g) 30 psu, (h) 37 psu, and (i) natural sea surface bubbles (photograph acquired in the Gran Canaria coast, reference size= 0.50 € coin, radius = 12 mm).

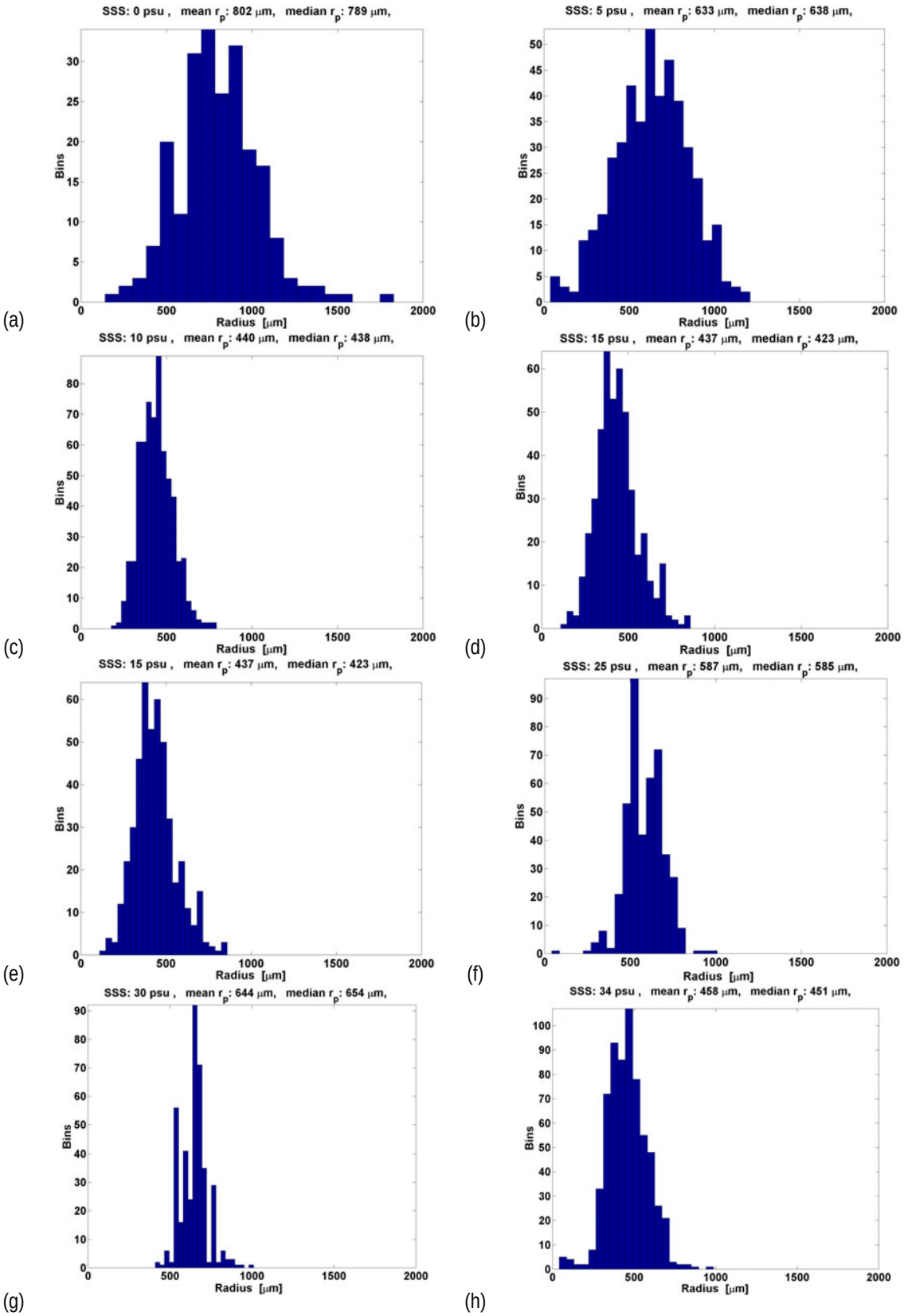

Figure 6.5. Distribution of bubbles radii at different salinities: (a) 0 psu, (b) 5 psu, (c) 10 psu, (d) 15 psu, (e) 20 psu, (f) 25 psu, (g) 30 psu, and (h) 34 psu.

In Figure 6.6a, the bubbles radii distribution from Gran Canaria coast pictures is shown. Figure 6.6b shows a Gamma pdf fit, adjusting the bubbles radii histogram. The “a” and “b” parameters of the best fit

Gamma distribution are a = 2.9 and b = 271.9. Note that the most probable bubbles radius is very similar to the radius of the Gamma pdf peak. The main difference as compared to Figures 6.5 is the longer tail corresponding to the large bubbles clearly seen in Figure 6.4i.

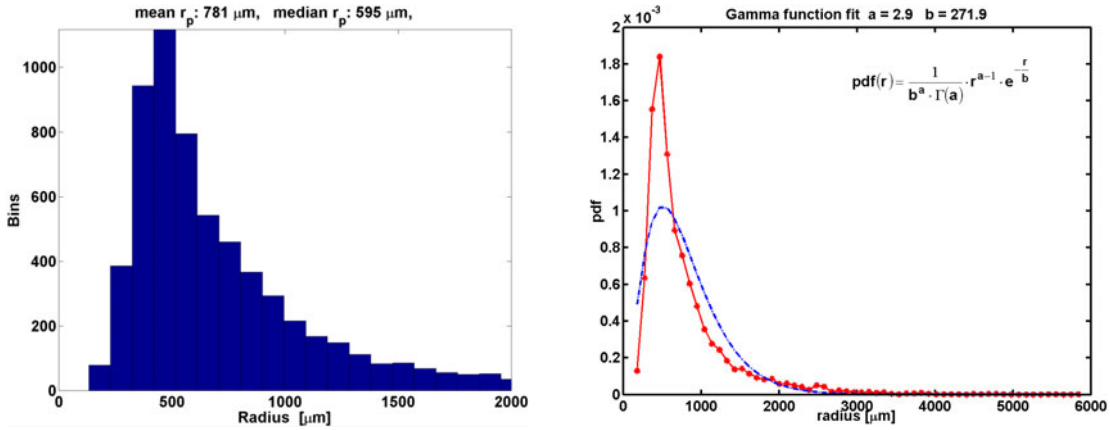

a) b)

Figure 6.6. (a) Distribution of the bubbles radii from Gran Canaria coast, and (b) bubbles radii from Gran Canaria coast/gamma distribution (red/blue and solid/dashed line).

VI.4.2.2 Foam layer thickness measurement

The foam layer thickness depends on the foam volumetric content. As it can be clearly seen in Figure 6.4, the thickness is mostly dependent on the salinity concentration and it increases with increasing salinity concentration. During the FROG campaign vertical foam profiles were analyzed to separate the main foam layer from the underlying water. In Figure 6.7a and Figure 6.7b this process can be shown. The mean value of the thickness layer is about 2.5 cm decreasing very close to 0 in the case of fresh water. This is clear observing the Figure 6.8a to Figure 6.8c.

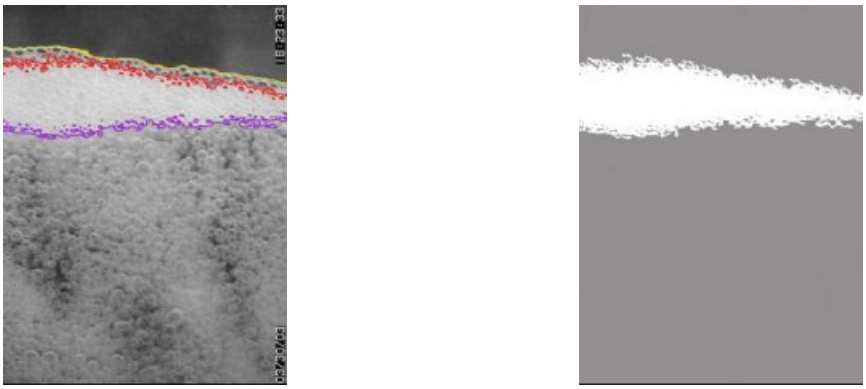

(a) (b)

Figure 6.7. (a) Different layers of a foam vertical profile, and (b) separation of the foam layer.

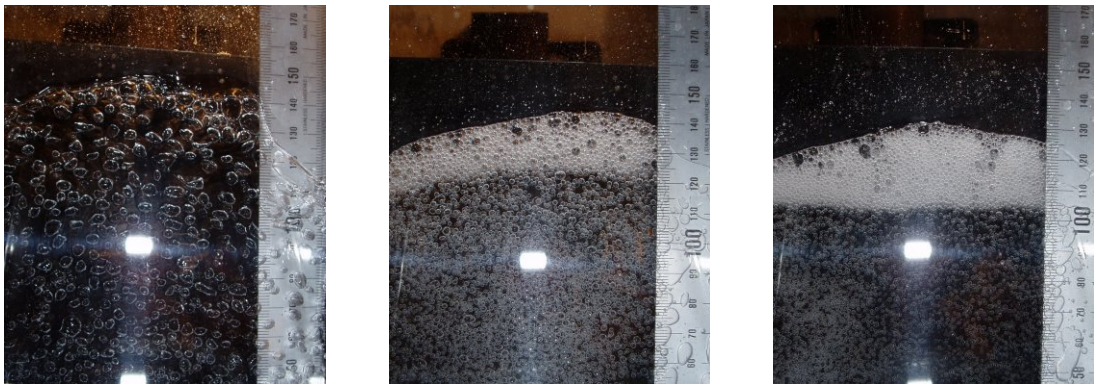

(a) (b) (c)

Figure 6.8. Three different foam vertical profiles: a) fresh water, b) SSS = 20 psu, and c) SSS = 37 psu.

VI.4.2.3 Void fraction beneath the foam layer

According to [25], the third parameter that contributes to the emissivity is the air-water fraction under the foam layer. Different tests performed at varying SSS from 0 to 37 psu, consisted of measuring the relative conductivity between the foam and the salty water. The Curtayne equation [17],

$$\sigma = \frac{1}{3}\left(\phi_l + \phi_l^{1.5} + \phi_l^2\right), \tag{6.19}$$

relates the liquid fraction (ϕ)and the water/foam conductivity (σ).

Hence, the void fraction beneath the foam layer f_a can written as:

$$f_a = 100 \cdot (1 - \phi_l). \tag{6.20}$$

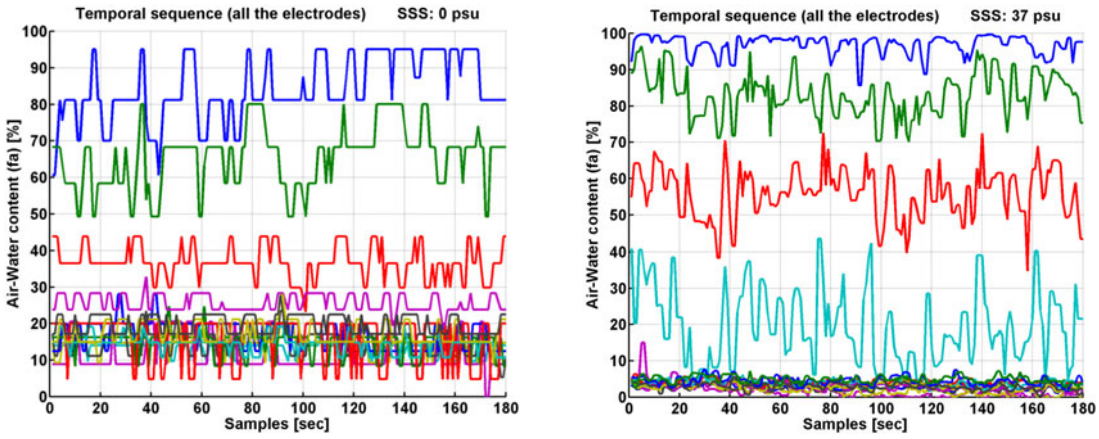

(a) (b)

Figure 6.9. Air-Water content (f_a) time sequence for every electrode a) SSS = 0 psu (15 electrodes, the top electrode was air), and b) SSS = 37 psu (16 electrodes).

In Figure 6.9a and Figure 6.9b the f_a time sequences of each electrode (maximum 16) at SSS = 0 psu and SSS = 37 psu are plotted. Although the number of bubbles is clearly smaller for fresh water than for salt water (Figure 6.8), their size is larger at SSS = 0 psu (Figure 6.5), and hence the air-water content

gradually increases. In Figure 6.10 the mean value of the 16 electrodes is presented at eight different salinities. It can observed that the void fraction beneath the foam layer is nearly constant and about 18% and 5% at SSS = 0 and 37 psu, respectively.

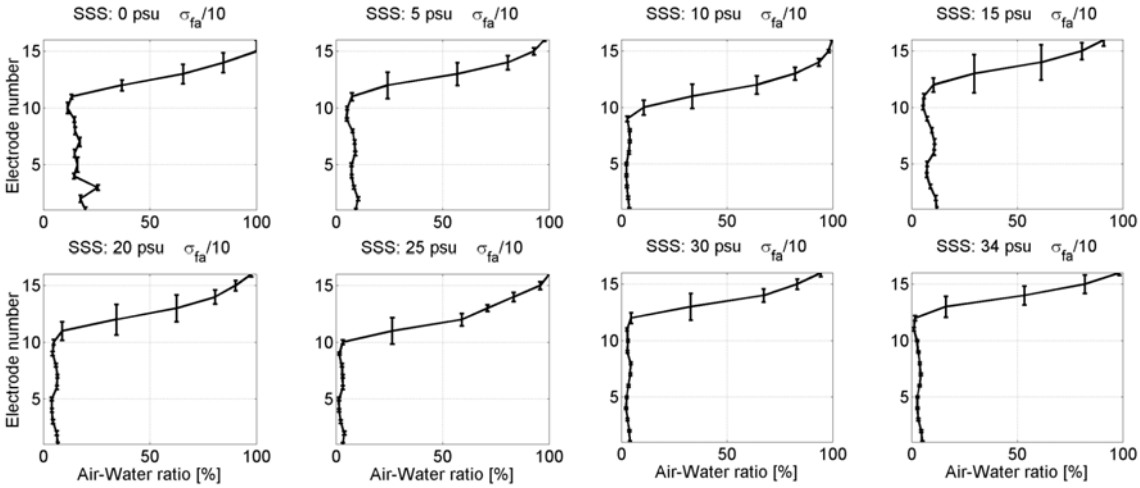

Figure 6.10. Air-Water fraction (f_a) mean value for every electrode at SSS = 0 to 34 psu. Each parallel golden electrode (3 mm x 4 mm, total 16) is separated 2 mm to the other. Element number 16 is located over the surface and hence the air-water ratio is 100 %.

VI.4.2.4 Main results on foam emission. Inter-comparison with the two-layer model

The measured sequences acquired during the FROG experiment at different incidence angles and salinities were converted into foam emissivities corresponding to a completely foam covered surface (eqn. (6.18)). In order to analyze the foam contribution into the emissivity, the foam-induced emissivities are considered, and can be expressed as (eqn. (6.21)).

$$\Delta e_{H,V} = e_{H,V}^{foam} - e_{H,V}^{foam-free}. \tag{6.21}$$

After the analysis of $\Delta e_{H,V}$, the following considerations have been taken into account:

- A normalized foam-induced emisivities by the foam thickness layer, is plotted as a function of the incidence angle (θ) and the salinity concentration at each sequence and polarization Figure 6.12a and Figure 6.12c,
- Some data points corresponding to low salinities (SSS < 5 psu) are not considered due to their high variability (due to foam thickness variability).
- To minimize the oscillations of the data points in Figure 6.12b Figure 6.12d the smoothed values are shown.

The main conclusions from the foam-induced emissivities are summarized in the following points:

- Assuming foam-free conditions (Figure 6.2), the SSS decrease contributes to increase the brightness temperature,
- The presence of foam increases the brightness temperature (Figure 6.3),
- The foam volumetric content (thickness) and the foam persistence is higher at high SSS,
- Figure 6.12 shows that the most important factor in the T_B increase is the foam thickness,
- The foam-induced emissivity due to the combination of the polarization and the incidence angle varies as follows: the brightness due to foam increases when the incidence angle increases, at V- polarization, and decreases with increasing incidence angle at H-polarization.

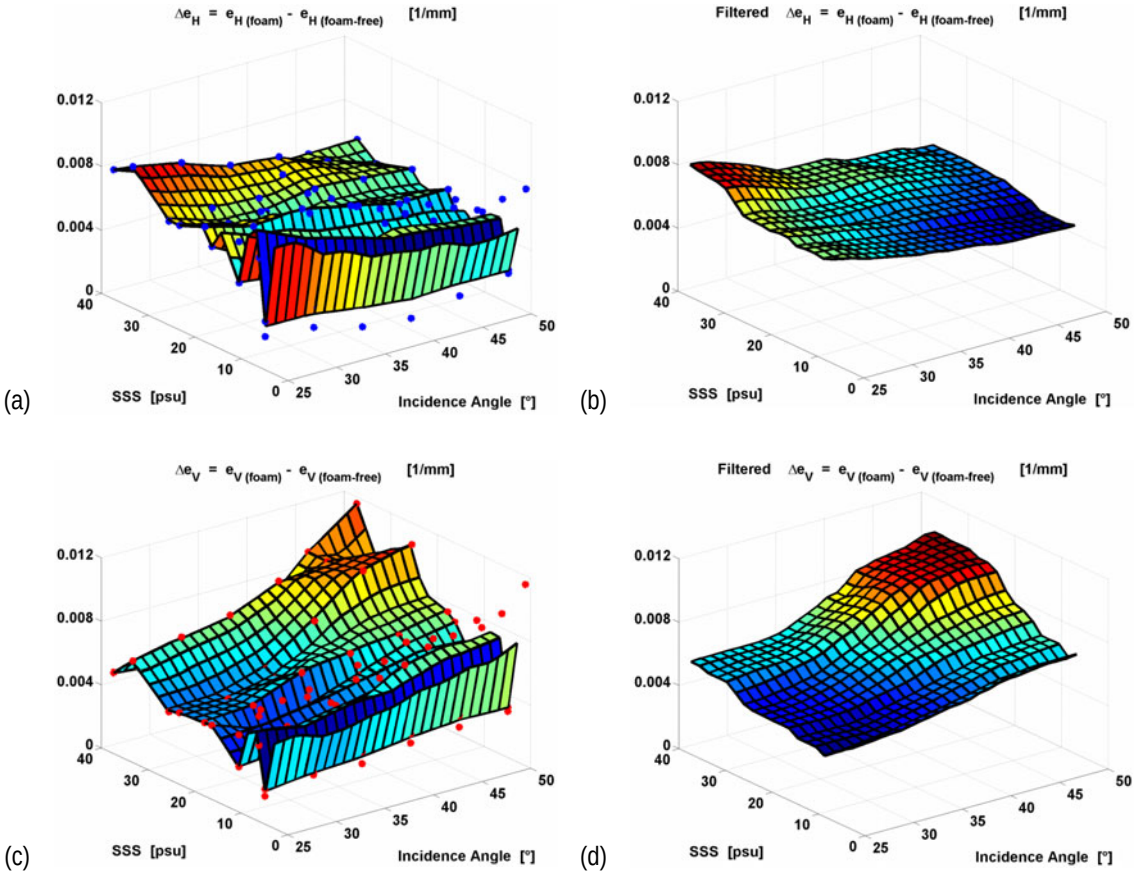

Figure 6.11. Induced emissivity (@100%) foam per mm at H- and V- polarizations as a function of the SSS and θ. (a) Measured data points (H- polarization), (b) same as Figure 6.11a, low pass filtered, (c) measured data points (V-polarization), and (d) same as Figure 6.11c low pass filtered.

Table 6.2 shows the foam-induced emissivity due to foam, normalized to the mean value of the foam layer thickness at H- and V- polarizations, and SSS = 37.3 psu.

Table 6.2. Foam-induced emissivity per mm of foam thickness at H- and V- polarizations SSS = 37.3 psu

Incidence angle θ [°]	25	30	35	40	45	50
$\frac{\Delta e_H(37.3\ psu)}{thickness}\cdot 10^{-3}\ \left[mm^{-1}\right]$	8.38	7.54	6.42	6.14	5.78	5.38
$\frac{\Delta e_V(37.3\ psu)}{thickness}\cdot 10^{-3}\ \left[mm^{-1}\right]$	5.86	5.91	6.3	7.67	9.15	9.82

The un-normalized sequence at high salinities (SSS = 37 psu) as a function of the incidence angle is presented in Figure 6.12. Data points are fitted by a polynomial (quadratic curve). The foam-induced emissivity as a function of the polarization and the incidence angle (°) can be expressed, as:

$$\Delta e_H^{foam}(\theta) \cong 1.132\cdot 10^{-4}\cdot\theta^2 - 9.595\cdot 10^{-3}\cdot\theta + 2.729\cdot 10^{-1} \quad @SSS = 37psu\ , \tag{6.22}$$

and,

$$\Delta e_V^{foam}(\theta) \cong 2.224\cdot 10^{-4}\cdot\theta^2 - 13.234\cdot 10^{-3}\cdot\theta + 2.567\cdot 10^{-1} \quad @SSS = 37psu\ . \tag{6.23}$$

with an rms error of $\sigma_H = 4.3\cdot 10^{-3}$, and $\sigma_V = 3.72\cdot 10^{-3}$ between the measurements and the fit.

The WISE-derived foam brightness temperature increase at U_{10} = 20 m/s is about 0.18 K [36] (extrapolated at θ = 0°). Extrapolating the foam-induced emissivity obtained in FROG campaign to nadir (0.00712 mm^{-1}), a SST of 16.5 °C, and the typical foam coverage of 1.5 % during WISE 2001 storm [36] the equivalent foam layer thickness should be approximately 6 mm.

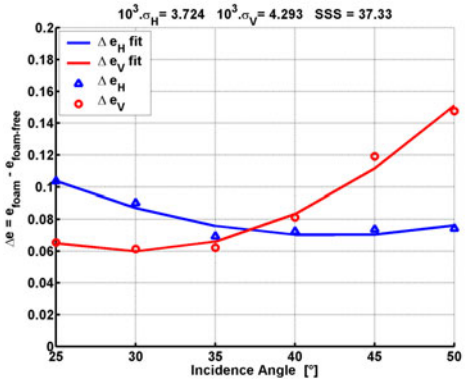

Figure 6.12. Foam-induced emissivity vs. incidence angle. Measured data points (H- (triangles, blue) / V- (circles, red)) polarizations, and their corresponding fits (solid line), (H (blue) / V (red)) polarizations.

The second goal of this work is to study the validity of the L-band foam emissivity model [25] by comparing it to the FROG measurements. For this reason, all the foam parameters required have been measured in FROG experiment. These were: radius bubbles (r_p), foam layer thickness, void fraction beneath the foam layer (f_a), and they have been presented in the previous sections. The bubble's water coating thickness is δ = 10μm derived from the high resolution pictures, which is similar to value used in [25]. The optimum stickiness factor is computed by fitting the measured sequences for different salinities

and the [25] model. Figure 6.13a to Figure 6.13c show the relationship between the measured sequences and the theoretical emissivities and a set of values of κ at H (blue) or V (red) polarizations at SSS = 5, 15 and 34 psu. The optimum value of κ chosen following the minimum Euclidean distance criterion, between H and V polarization, to minimize the overall rms error. Table 6.3 shows the different values of the stickyness factor corresponding to different salinities, at both polarizations. As expected, it increases with increasing salinity. However, κ should be the same at both polarizations. The reason for this small difference is not known. The optimum values of κ are shown in the first and the second column respectively. In the third column the optimum value of κ is shown, chosen following the minimum Euclidean distance criterion.

(a) 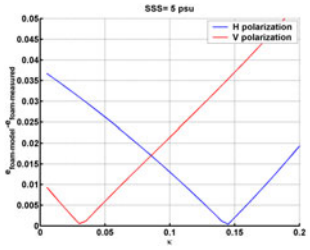

(b) 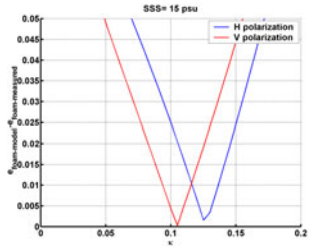

(c) 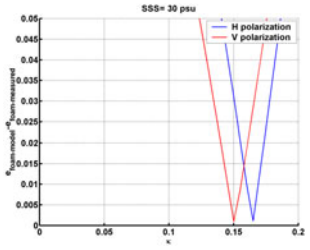

Figure 6.13. Values of κ that minimize the measure sequences and the theoretical model [25] at (a) 5 psu, (b) 15 psu, and (c) 30 psu.

Table 6.3. Estimated Stickiness factor κ, fitting the measures to the theoretical model

SSS	Optimum κ (H- polarization)	Optimum κ (V- polarization)	Optimum κ
5	0.14	0.03	0.08
10	0.10	0.04	0.07
15	0.13	0.11	0.12
20	0.13	0.12	0.12
25	0.17	0.15	0.16
30	0.17	0.15	0.16
34	0.21	0.17	0.19

The emissivity curves at H- and V- polarizations for different salinities are plotted Figure 6.14a to Figure 6.14h. Each figure contains the measured emissivity curves (with and without foam) at both polarizations, and the theoretical curve obtained after applying the model [25]. The rms error between the measured and the theoretical foam emissivity curves is also shown in each figure ($\sigma_{\Delta H}$, $\sigma_{\Delta V}$).

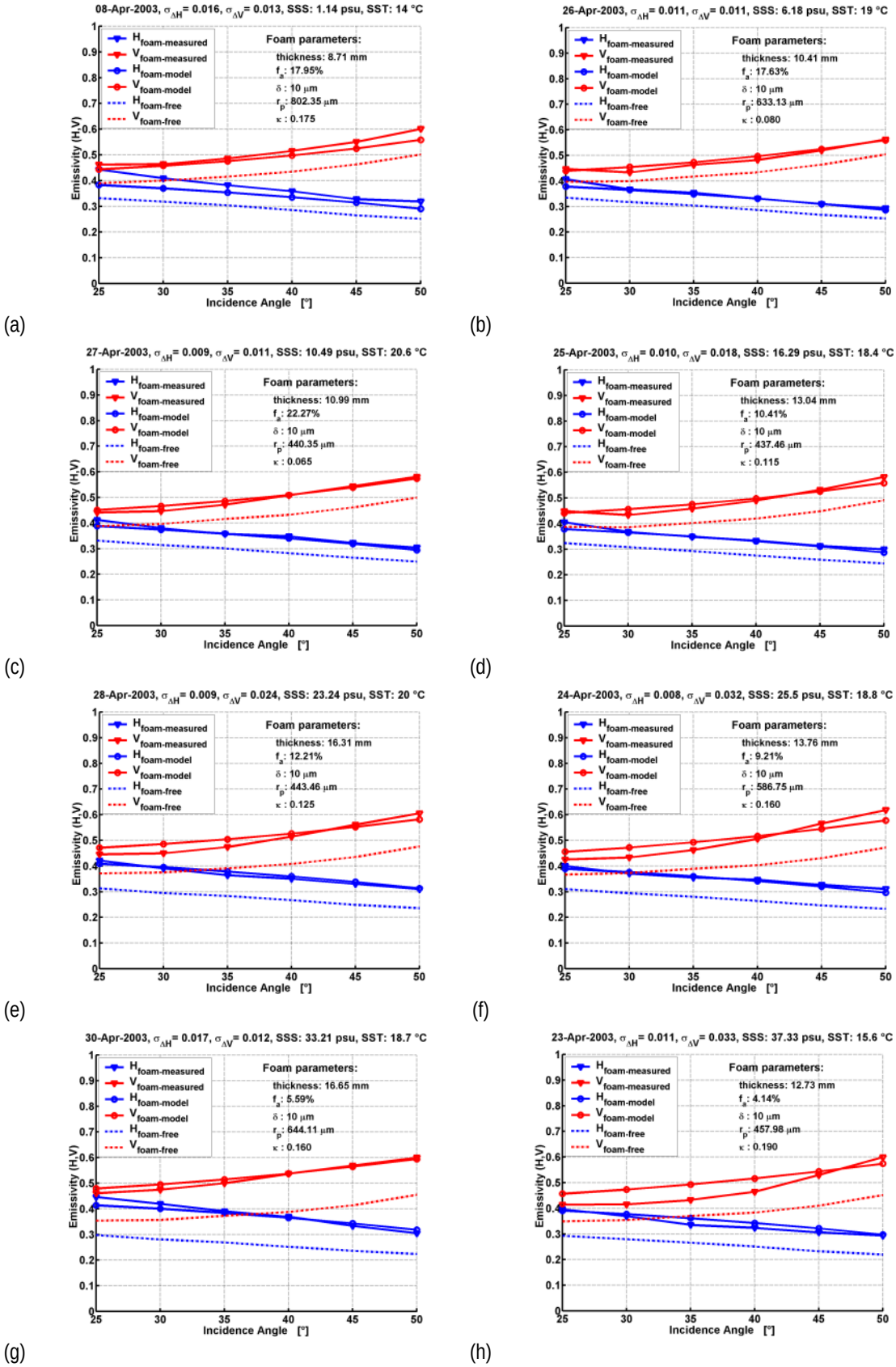

Figure 6.14. Emissivities at H- (blue) and V- (red) polarizations for different salinities. The dashed lines indicate foam-free conditions. The solid line marked with circles indicates the measures taken during FROG campaign and the solid line marked with triangles the theoretical model taken into account some measured parameters: thickness, bubbles radii and f_a, δ=10μm, and the optimum κ value after fitting the emissivity measures and the theoretical model.

VI.5 Rain contribution to the T_B measurement

The objective of this part of the experiment was to observe and quantify the contribution of the rain-induced surface roughness in the T_B measurements at L-band.

VI.5.1 Experimentally-derived rain-perturbed water T_B

It is know that the effect of the rain-induced surface roughness on T_B is very small [50]. Therefore, the brightness temperature difference measured with LAURA's radiometer at H- and V- polarizations is very close to zero (Figure 6.15a), even at an artificial-generated rain rate of Q ~ 4000 mm/h for all the incidence angles. The measurement sequence consisted of measuring the T_B at each incidence angle, following the next sequence: no rain (2') – rain (2') – no rain (2'). The last sequence was not taken into account, since it is a transient regime in which the pipes were still filling out. Moreover, the transient samples at the beginning of the rain generation were not considered either to compute the emissivity. The differential measurement $e_{H,V}^{rain} - e_{H,V}^{no\ rain}$ was performed and plotted in the same figure.

Figure 6.15b shows the emissivity at H- and V- polarizations without and with rain presence, and the numerical values are presented in Table 6.4. The induced T_B is about 2 K at T_{phys} = 21° C, and Q ~ 4000 mm/h. The induced brightness temperature increases at V- polarization, and decreases at H-polarization with the incidence angle.

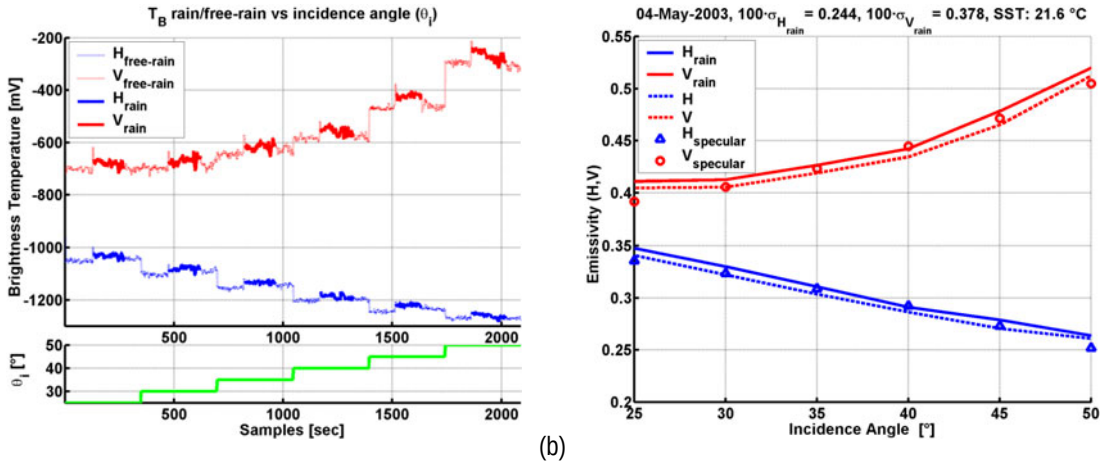

(a) (b)

Figure 6.15. (a) T_B raw data (mV) with/without rainfall presence (solid line/dotted line) at the H- and V- polarizations for θ_i = 25° to 50 °, and (b) emissivity measured at H- (blue) and V- polarization (red) versus the incidence angle taking into account rainfall (solid line), free-rain (dotted line), and the specular water surface theoretical model (blue/red triangles/circles).

Table 6.4. Emissivity vs θ_i polarization and presence or absence of rain.

Incidence angle θ [°]	25 (rain-free)	50 (rain-free)	25 (4000 mm/h)	50 (4000 mm/h)
e_H	0.341	0.261	0.348	0.264
e_V	0.405	0.512	0.411	0.520

In Figure 6.16a and Figure 6.16b a zoom of the temporal data sequence collected by the picolog ADC12 (water roughness meter) is plotted. The signal frequency variability is 3.2 Hz and it is associated to the roughed water surface due to the splashing rain (Figure 6.16a, temporal domain, Figure 6.15c and Figure 6.16d, frequency domain). On the other hand, a slow oscillation very close to 0.1 Hz is observed, due to the dynamic behavior of the water inside the pool (Figure 6.16b, temporal domain).

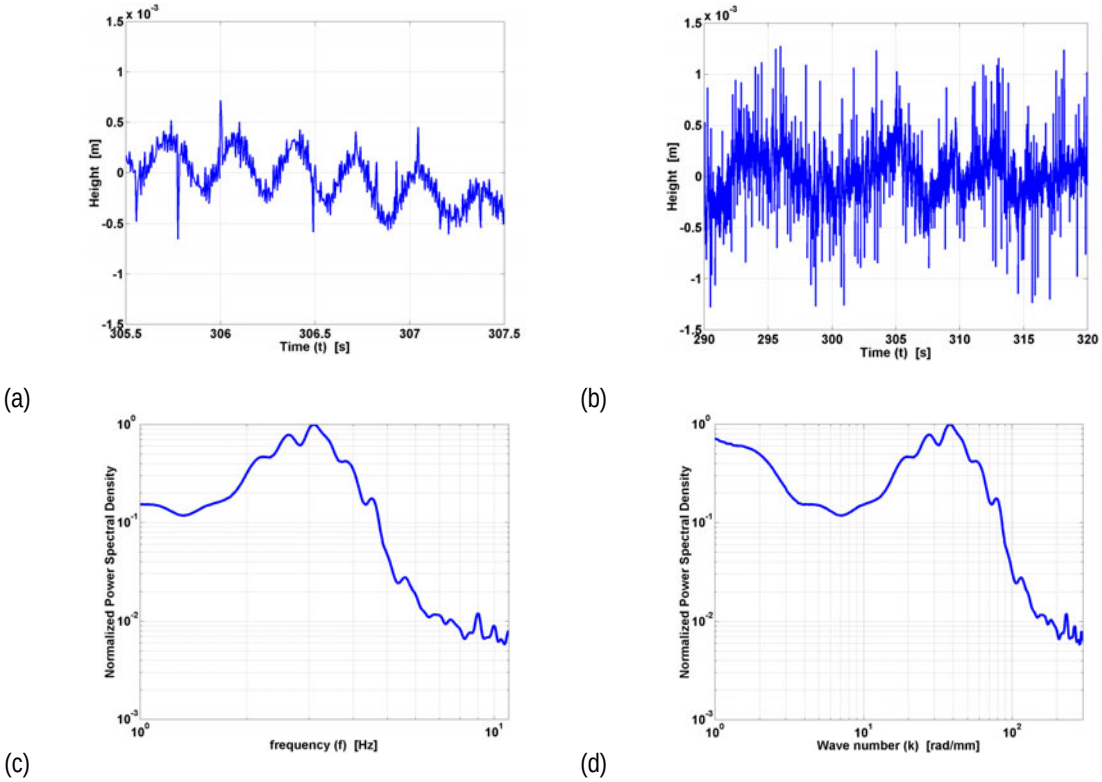

Figure 6.16. (a) Temporal data sequence associated to the roughness water surface, (b) slow oscillation due to the dynamic behavior of the water inside the pool, (c) normalized power spectral density vs. frequency of Figure 6.16a, (d) normalized power spectral density vs. wave number of Figure 6.16a.

As seen in Figure 6.15b, the induced brightness increases at V- polarization, and decrease at H-polarization with the incidence angle. These results are in excellent agreement with the brightness temperature simulations, computed with the Small Slope Approximation (SSA) method [51] (Figure 6.17a and Figure 6.17b)

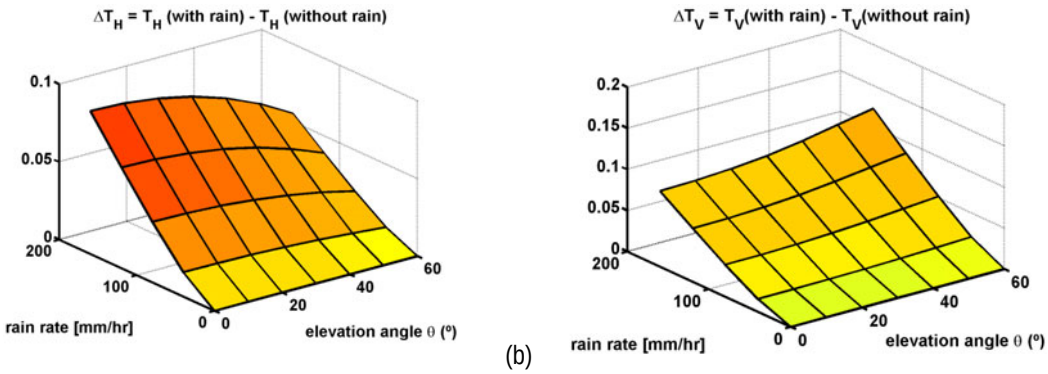

Figure 6.17. T_B change due to the presence of rain computed with SSA model (a) H-, and (b) V- polarization [51].

In Table 6.5, the rain-induced emissivities measured during FROG campaign at H- and V-polarizations are shown. The data at 45° incidence angle is abnormally high, no reason has been found. In Figure 6.18 the rain-induced emissivity at H- and V- polarizations is plotted, and fitted by a polynomial of degree 2.

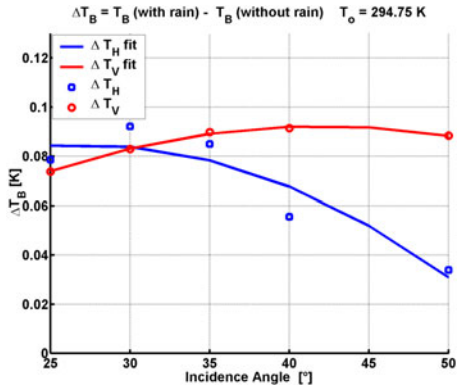

Figure 6.18. Rain-induced emissivity at H- (blue, squares) and V- (red, circles) polarizations. Measurements are fitted by a polynomial of degree 2, excluding the 45° point. Rain rate is scaled to 160 mm/h.

Table 6.5. Brightness temperature change due to the presence of rainfall scaled to 160 mm/h.

Incidence angle θ		25°	30°	35°	40°	45°	50°
$\Delta T_H = T_{H(\text{with rain})} - T_{H(\text{without rain})}$	[K]	0.0786	0.0921	0.0849	0.0555	0.0958	0.0339
$\Delta T_V = T_{V(\text{with rain})} - T_{V(\text{without rain})}$	[K]	0.0738	0.0829	0.0899	0.0914	0.1535	0.0884

VI.6 Oil slicks contribution to the T_B measurement

A sinusoidal variations of T_B are produced with the presence of oil slicks, since this element acts as a matching layer between water and air. The amplitude of the variations depends mainly on the oil slick thickness, the maximum and minimum values are separated one quarter of wavelength as it was shown in Figure 6.19. It can be observed that the maximum T_B variations (oil thickness ~15 mm to 25 mm) at L-band is ~ 6 K/mm at θ = 0° according to the model.

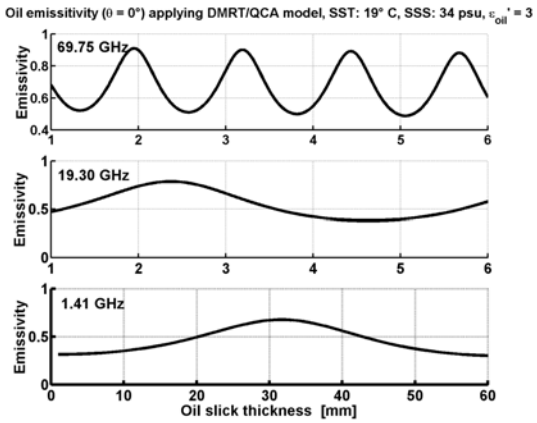

Figure 6.19. Theoretically emissivity variation at nadir vs the oil slicks thickness at three different frequencies applying DMRT/QCA (Dense Media Radiative Transfer theory/Quasy Crystalline Approximation)[24].

VI.6.1 Experimentally-derived oil slicks T_B

The main goal of this experiment was to analyze the contribution to T_B at L-band of a very thin (47μm) oil film over the water (oil slick). For this purpose, 1 litter of mineral oil was poured over the pool surface. Results are presented in Figure 6.20 and show the measured emissivity (solid line) at H-polarization (blue)/ V- polarization (red) versus the theoretical emissivity using the theoretical model (dashed line) at the two polarizations (consisting of computing the emissivity of two homogeneous layers, oil and water). Differences are within the calibration errors of the two consecutive measurements. According to the oil slicks FROG measurements and, observing the theoretical model (Figure 6.20), it seems clear that the contribution of the oil slicks in the brightness temperature at L-band is very small.

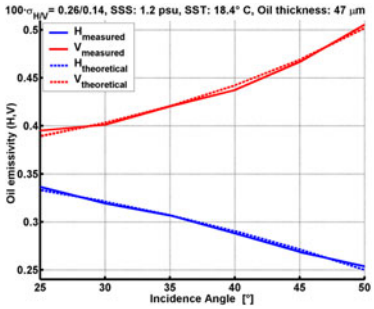

Figure 6.20. Measured (solid) vs theoretical (dashed) emissivity at H- polarization (blue) and V- polarization (red).

VI.7 Conclusions

By observing the FROG field experiment results it can be appreciate that:

- Foam contributes in the brightness temperature T_B increase at L-band.
- The foam-induced T_B increases at vertical polarization and decreases at horizontal polarization with the increase of the incidence angle (θ = 25° to 50°).
- Foam formations are thicker at high salinity concentrations than at fresh water. Hence, the T_B increases more for salty water.
- All the parameters of the two-layer theoretical model [25], have been measured: the foam layer thickness, the radii bubbles distribution, the air-water fraction beneath the foam layer, and the water bubble content, and the sticky factor estimated comparing the measures and the theoretical model. Measurements are in good agreement with the theoretical model at H-polarization and are slightly under estimated at V-polarization
- At L-band the rainfall contribution to T_B is clearly smaller than the foam contribution and negligible for all practical purposes except for: the formation of fresh water layer, and the dumping of the large waves.
- The FROG experimental results show a T_B increasing at H- and V- polarization due to the rainfall. A brightness decrease at H- polarization with the increasing of θ is produced, at the

same manner than the theoretical model [51], computed with the Small Slope Approximation (SSA) method.

- In FROG 2003, the increasing of T_B due to the oil slicks can be neglected.